Six smart guidelines for high-tech manufacture on low-tech 3D printers the case of the 3Flex

Trauzettel, Fabian; Vander Poorten, Emmanuel; Ourak, Mouloud; Dankelman, Jenny; Breedveld, Paul

DOI
10.1080/09544828.2024.2322169

Publication date
2024

Document Version
Final published version

Published in
Journal of Engineering Design

Journal of Engineering Design

ISSN: (Print) (Online) Journal homepage: www.tandfonline.com/journals/cjen20

Six smart guidelines for high-tech manufacture on low-tech 3D printers: the case of the 3Flex

Fabian Trauzettel, Emmanuel Vander Poorten, Mouloud Ourak, Jenny Dankelman & Paul Breedveld

To cite this article: Fabian Trauzettel, Emmanuel Vander Poorten, Mouloud Ourak, Jenny Dankelman & Paul Breedveld (2024) Six smart guidelines for high-tech manufacture on low-tech 3D printers: the case of the 3Flex, Journal of Engineering Design, 35:6, 665-684, DOI: 10.1080/09544828.2024.2322169

To link to this article: https://doi.org/10.1080/09544828.2024.2322169

Published online: 13 Mar 2024.

JOURNAL OF ENGINEERING DESIGN
2024, VOL. 35, NO. 6, 665–684
https://doi.org/10.1080/09544828.2024.2322169

Taylor & Francis
Taylor & Francis Group

Six smart guidelines for high-tech manufacture on low-tech 3D printers: the case of the 3Flex

Fabian Trauzettel[a,b], Emmanuel Vander Poorten[b], Mouloud Ourak[b], Jenny Dankelman[a] and Paul Breedveld[a]

[a]Faculty of Mechanical Engineering, Department of BioMechanical Engineering, Delft University of Technology, Delft, The Netherlands; [b]Department of Mechanical Engineering, Division PMA, Katholieke Universiteit Leuven, Heverlee – Leuven, Belgium

ABSTRACT

While articulated surgical instruments have enabled the proliferation of minimally invasive interventions, procedures such as laparo-endoscopic single-site surgery are waning in popularity. One potential reason for this decline is a lack of sufficiently dexterous instruments. Although multi-steerable instruments exist, these are often complex and therefore expensive assemblies. Even when 3D printing was used to simplify the design of these instruments, the requirement for high-performance 3D printers limited the reduction in manufacturing costs. To tackle this issue, we propose six guidelines for converting a 3D printed compliant medical instrument from printing on a Digital Light Processing (DLP) printer to a Fused Filament Fabrication (FFF) printer. These guidelines provide a framework to manage and compensate for differences in the two processes to achieve comparable results at a reduced cost. The proposed guidelines were evaluated by assembling a FFF 3D printed prototype that shows equivalent performance to its DLP 3D printed counterpart.

ARTICLE HISTORY
Received 4 April 2023
Accepted 19 February 2024

KEYWORDS
Hyper-redundant; 3D printing; medical devices; snake-like; surgical instruments

1. Introduction

1.1. Background

Minimally-Invasive Interventions (MIIs) have become widespread over the last few decades due to shorter hospital stays, faster recovery, reduced scarring and less pain (Mohiuddin and Swanson 2013). A driver behind the advancement of MIIs has been the evolution of minimally invasive instruments from rigid to articulated, giving clinicians greater dexterity in the human body. Nevertheless, approaches such as LaparoEndoscopic Single-site Surgery (LESS) are waning in popularity, primarily due to concerns over safety and efficacy. Sorokin et al. (2017) argue that this trend could be reversed by improved, more dextrous, instruments.

The current generation of articulated surgical instruments generally articulate at the wrist, like the FlexDex (Vliet et al. 2022), LaproFlex (Scheltes 2019), or EndoWrist (Teoh

CONTACT Fabian Trauzettel f.trauzettel@tudelft.nl Department of BioMechanical Engineering, Faculty of Mechanical Engineering, Mekelweg 2, 2628CD Delft, the Netherlands

et al. 2018). To increase the dexterity of these instruments, multiple joints can be added to the shaft of the device to permit articulation at multiple points, creating a multi-steerable device. Multi-steerable devices are being developed to navigate in tortuous anatomy, or even advance through the body using Follow-The-Leader (FTL) motion, where the shaft of the instrument follows the path taking by its tip, like a snake weaving around obstacles (Henselmans et al. 2020).

A number of multi-steerable FTL motion systems exist targeting medical applications, ranging from highly experimental to commercially available (Culmone, Yikilmaz, et al. 2021). While these devices are more dexterous than their wrist-articulated counterparts, this improvement comes at the cost of complexity; these devices tend to be intricate arrangements of complex frame elements and compliant segments, even sometimes featuring built-in piezoelectrics or complicated brake mechanisms.

3D printing non-assembly and compliant structures presents a way to combat rising complexity in these designs. For example, Ai et al. (2021) propose a tendon-driven shaft for bronchoscopic applications with a 3 mm outer diameter. The prototype was printed on an EnvisionTec Perfactory P4K (EnvisionTec GmbH, Gladbeck, Germany), a Digital Light Processing (DLP)-type 3D printer, and features many compliant joints. Each joint permits a different amount of bending, allowing the shaft as a whole to achieve anisotropic bending curves which are better suited to navigating the lung than simple continuous curves. Conventionally manufacturing this design would require many discrete parts, each with different dimensions and requiring precise assembly. Wu et al. (2023) published a segmented flexible manipulator for minimally invasive surgery with a 15mm outer diameter and printed on an unspecified Stereolithography (SLA) machine in an unnamed resin. Their design consists of a series of discrete, ball-and-socket joints which were assembled after printing.

Similarly, Culmone, Lussenburg, et al. (2021) designed a laparoscopic grasper with a wrist that is steerable in two Degrees of Freedom (DOF). The device features a shaft diameter of 8 mm and consists of just five parts which snap together. The design is fully 3D printed on a Formlabs Form 3B (Formlabs, Somerville, MA, USA), an SLA 3D printer. The low part count here is achieved by consolidating the functionalities of multiple components into fewer, multi-functional parts, a strategy enabled by 3D printing.

Krieger et al. (2017) take this concept to the extreme by using an EOS (EOS GmbH, Krailling, Germany) Nylon Powder Bed Fusion (PBF) machine to create a large, compliant overtube robot for natural orifice surgery in just two pieces. Similarly, Song et al. (2023) propose an endoscopic overtube robot manufactured in PA12 Nylon on an unnamed PBF machine. Wang et al. (2023) present a flexible robotic laparoscope with an articulated section 3D printed on an unspecified PBF machine and in an unspecified nylon material.

By using multi-material Drop-On-Demand (DOD) photopolymer jetting on a Stratasys J735 (Stratasys Ltd., Rehovot, Israel), Lin et al. (2021) were able to create a magnetically-steered robot catheter with a diameter of just two mm. By leveraging multi-material printing to create a stiffer and a more flexible segment of the catheter, their design can achieve S-shaped curves, whereas conventional designs are only capable of steering in C-curves. This paper also represents the only paper found in our search which leveraged multi-material printing to directly print catheters.

These examples all leverage comparatively high-performance and therefore expensive 3D printing processes with printers routinely costing upwards of tens of thousands of

euros, making them available only to the businesses or particularly well-equipped research groups. By comparison, Fused Filament Fabrication (FFF) is a much more affordable 3D printing process that is both inexpensive and flexible. While FFF has been used to create sophisticated flexible and articulated medical instruments, the published designs seem to simply utilise FFF as a process of convenience rather than incorporating its specific advantages into the design.

Hernández-Valderrama et al. (2022) propose a laparoscopic instrument with an FFF-printed articulated wrist capable of steering in two DOF, and Hwang and Kwon (2020) present an overtube robot utilising FFF printed rolling joints for articulation. In both cases, the articulating structure consists of many individually printed segments that appear to be manually assembled, thereby negating the potential for minimum- or non-assembly strategies provided by 3D printing. As a result, the manufacturing savings from implementing 3D printing in these devices is still limited.

1.2. Case study: HelicoFlex

1.2.1. 3D printed multi-steerable surgical device

For the purposes of this work, it was decided to modify the HelicoFlex design developed by Culmone et al. (2020) to permit printing on a commonly-available FFF 3D printer. The HelicoFlex is a multi-steerable instrument pictured in Figure 1 and was manufactured on a Perfactory 4 Mini XL, a Digital Light Processing (DLP) 3D printer. This design presented a leap forward as it comprised only three frame parts; comparable non-printed devices usually have part counts in the dozens. The HelicoFlex is printed in three pieces: the multi-steerable shaft, the handle with converging section, and an end cap. The pieces are printed vertically in the build volume of the Perfactory 4 Mini XL and are engineered so that they permanently press-fit into each other after the tendons have been threaded through the shaft.

Functionally, the prototype consists of three main sections; the compliant handle (Figure 1(a), left), a converging section (Figure 1(a), middle), and the multi-steerable shaft (Figure 1(a), right). The handle of the instrument and the tip are connected to each other via the tendons of the instrument. Bending the handle will make the tip to mirror the user's input on the handle, i.e. if the user bends the handle upward, the shaft will bend downward.

1.2.2. HelicoFlex prototype

The shaft of the HelicoFlex prototype, shown in Figure 1(a), possesses an outer diameter of eight mm, and four channels of 1.75 mm diameter. The shaft is 180 mm long and comprises a 120 mm proximal rigid section and five individually steerable segments with a combined length of 60 mm. Each of the steerable segments features bending articulation in two DOF, for a total of ten DOF. Each segment comprises a 1 mm diameter coaxial backbone surrounded by four intertwined helicoids. Together, the helicoids and the backbone form a compliant structure that is stiff in torsion and axial compression but allows for low bending stiffness. The tendons of the instrument are attached by looping them through tendon attachment grooves in the outer face of the shaft before leading them back through channels in the shaft. By attaching four tendons to the distal ends of each of the five segments it is possible to control the deflection and the direction of bending at the tip of the instrument (Culmone et al. 2020) with a total of 20 tendons.

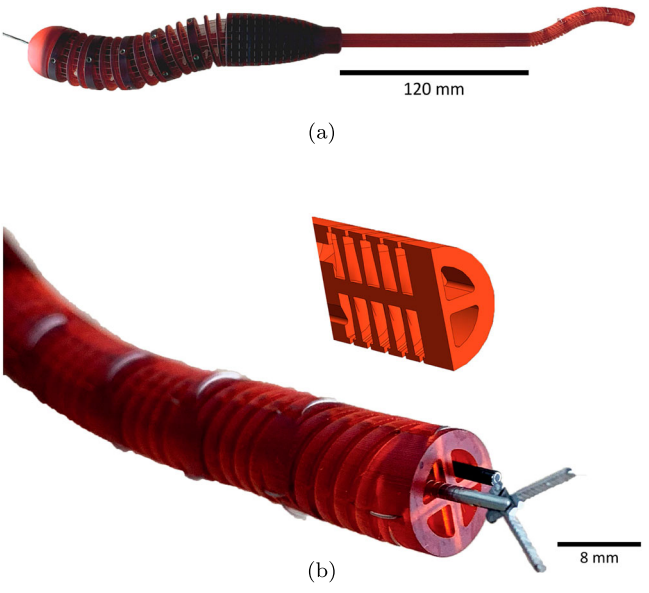

Figure 1. Photographs of the HelicoFlex prototype developed by Culmone et al. showing an overview of the assembled prototype (a) and a closeup of the instrument shaft (b). (b) also shows a cutaway of the most distal shaft segment, exposing the internal 'T' shaped cross-section of the helicoids. The shaft has a diameter of 8 mm. Figures adapted from Culmone et al. (2020).

1.2.3. Room for improvement

While the HelicoFlex solves many complexities around manufacturing multi-steerable medical instruments, some issues remain to be solved. The HelicoFlex is a tendon-driven design that requires four tendons per segment. Each tendon is housed in its own channel, meaning the shaft must accommodate 20 channels, each with a diameter of 0.45 mm. Resolving so many small features is difficult for most 3D printers, precluding the design from printing on more affordable, lower precision 3D printers. Furthermore, while the printer used in the HelicoFlex project was able to resolve the tendon channels using non-biocompatible resins, they clogged with the use of more viscous biocompatible resins, so a non-biocompatible photopolymer resin was used to manufacture the HelicoFlex prototype.

The above examples show that, while complex articulation mechanisms in medical devices can be simplified using 3D printing, the approach used in the HelicoFlex project relies on the use of high-resolution, and therefore expensive, 3D printers. As FFF 3D printers have become less expensive over the last decade and therefore have become much more available, being able to manufacture multi-steerable devices on such 3D printers could promote the use of multi-steerable medical devices as the manufacturing cost is lowered.

1.3. Goal of this research

The goal of this study is to share the design knowledge gained from converting a design that is only printable on expensive Digital Light Processing (DLP) 3D printers to printing on more cost-effective FFF printers. This know-how is distilled into a set of six design guidelines for the low-cost manufacture of advanced, compliant, multi-steerable medical instruments using affordable FFF 3D printers.

2. Materials and methods

2.1. Materials

The 3D printer used in this project is a Prusa i3 MK3S (Prusa Research a.s., Prague, Czechia). While not the most affordable FFF 3D printer on the market, it is one of the most common, with an estimated market share of 10% in 2022 (Josef Prusa acquires US-based company Printed Solid, Inc. 2022). With a sub-€1000 price tag it lies within reach of most hobbyists and almost all research facilities worldwide.

As many features being printed in this project are less than 1 mm in size, the default ⌀0.4 mm nozzle was replaced with a ⌀0.25 mm nozzle (E3D-Online Ltd, Chalgrove, UK). This upgrade cost £7.50 excluding tax and shipping.

All designs created for this study were created using Autodesk Inventor 2022 (Autodesk, Inc., San Rafael, CA, USA), converted into an.stl file and sliced using PrusaSlicer 2.4.2 (Prusa Research a.s., Prague, Czechia) to generate a g-code file. All parts were printed using AmazonBasics blue Polylactic Acid (PLA). While this filament is not biocompatible, PLA as a polymer is used in resorbable medical applications (Lou et al. 2008).

2.2. Methods

As 3D printing is a prototyping process, a trial-and-error approach was followed to print the HelicoFlex design using the FFF process. First, the original HelicoFlex design was imported into PrusaSlicer and sliced using the default settings for a Prusa i3 MK3s using 0.15 mm layers and the ⌀0.25 mm nozzle. If the print failed, the problem causing the failure was diagnosed and the design was modified to prevent the failure from reoccurring. The insights gained from the failed 3D prints were implemented in the final design of the Fused Filament Fabricated Flexible instrument – the 3Flex.

3. Design process

3.1. Achieving a completed print

Problem: Vertically not printable

The Prusa i3 MK3s uses a motion system layout where the print bed moves along the *Y*-axis and the nozzle moves along the *X* and *Z* axes. The print bed moves with high accelerations, up to 1000 mm/s^2. Printing the HelicoFlex standing upright on the Prusa, the same orientation as on the EnvisionTec, resulted in the print quality degrading as the print progressed. Stray material collected on the top of the print as the print quality degraded due to the acceleration of the print bed and the nozzle collided with it, leading to the object losing print bed adhesion and failing.

Solution: Sticking it horizontally

In cases such as this one, the HelicoFlex presents a worst case scenario for this type of printer. Not only is the amount of contact between the object being printed and the bed of the printer small, but the object itself is quite tall in the Z-axis, making it maximally sensitive to the movements of the print bed.

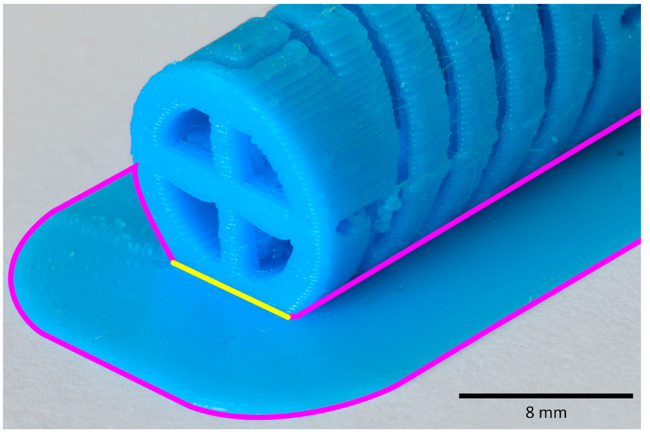

Figure 2. HelicoFlex segment printed horizontally on the print bed with the addition of a flat side (yellow line) and brim (surrounded by a magenta outline). The brim is an expansion of the first print layer that helps the segment remain attached to the print bed.

The first step to address these issues is to simply lay the object flat on the print bed to reduce the effect of print bed acceleration. In cases where the object has a flat geometry on its side, both issues are now solved: there is likely greater contact with the print bed, and the object will likely be shorter in the *Z*-axis, improving the odds of a successful prints. The HelicoFlex, however, has a cylindrical cross section. Laying it flat on the print bed will not improve the situation significantly as the only contact between the object and the print bed is a single line. There are only two ways to ensure adhesion for round parts: add support material to stabilise the print, which will result in poor surface finish and lost resolution on the underside of the print, or increase the contact area by designing the shaft with a flat side. As it was deemed that adding a flat side would not affect the functionality of the design, 0.5mm of material on one side of the shaft was removed, creating a flat side to increase the surface area of object in contact with the print bed.

While this improved results, it was still impossible to achieve a complete print. The helicoids are sliced parallel to the print bed, creating 'islands' – sections of a layer that are disconnected from the rest of the part. These islands easily lose adhesion and separate from the rest of the part, causing the flexible section of the HelicoFlex shaft to fail. To prevent this, a brim was added to the object to connect the islands and to increase the print bed contact area even further. A brim consists of material that is extruded in loops around the footprint of the object to be printed. This material does not belong to the object itself; it merely serves to increase the contact area of the object being printed and is intended to be removed in post processing.

The addition of the brim resulted in a 3D print (see Figure 2) that, while still flawed in several areas and non-functional, was structurally intact at the end of the printing process.

3.2. Finding optimal bed adhesion

Problem: Too much adhesion

For small objects such as the flexible shaft being printed here, it can be difficult to manage the correct amount of bed adhesion. While the addition of a brim to the part resulted in an

intact print, the resulting object did not possess the desired functionality; the brim material had fused together with the part, preventing the shaft from flexing as designed. Mechanically cutting away the brim restored a minimal amount of function, but the part was not usable.

Brim-object fusion could be avoided by modifying the 'brim separation gap' setting in PrusaSlicer, which creates a small space between the object and the brim. However, increasing this value immediately led to a resurgence of the adhesion loss problem. While it is likely that some sweet-spot separation between brim and object could be found by trial and error, this is time consuming and will constantly require adjusting as the distance between the printer nozzle and print bed will vary from print to print, and will drift over time.

Solution: From print bed to print lines

In FFF 3D printing, a raft is another type of support structure used to improve first layer adhesion. While a brim is printed around an object as the first layer is printed, a raft sits between the print bed and the object itself so the object sits on a larger piece of printed material. The right amount of bed adhesion can be achieved by using specific raft settings that allow the object to remain adhered during the print, while also being removable without damaging it and leave as little residue on the part as possible.

Default raft settings on slicers such as Cura or PrusSlicer will simply create a raft consisting of two to three solid layers and then place the object floating in the air above the surface of the raft. This prevents the first layer of the object from being completely fused to the raft, and results in a more removable raft, as the material in the first object layer has a small amount of time to cool as it drops from the nozzle through a small distance of air before contacting the raft. For parts with such small features as the HelicoFlex, the loss in position accuracy from this small drop can cause individual helicoids to fall over during printing, meaning that while the object as a whole remains adhered to the print bed, individual helicoids will have broken off during the print and the resulting object will be non-functional.

A good raft structure for delicate structures like the HelicoFlex comprises a solid first layer for maximum bed adhesion, and an interface layer that connects the object and the raft. The interface layer possesses a series of individual extrusion lines spaced 0.65 mm apart and angled at 45° to the axis of the shaft being printed. Unlike a conventional raft, there should be no air gap between the interface layer and the object itself – this allows for acceptable lower surface quality, while the raft can easily be removed from the object leaving only the interface lines, which can be quickly scraped off using a blade. While there can be residual lines from the interface layer adhering to the underside of the segment, they do not interfere with the segment actuation. The resulting print is shown in Figure 3.

3.3. Managing overhangs

Problem: Steep helix angle

The shaft of the HelicoFlex design consist of four helicoids intertwined with each other (Culmone et al. 2020). Each instance completes only one turn about the backbone of the structure, meaning it possesses a rather steep helix angle (see Figure 4(a), top). This steep helix angle creates an overhang, which increases the difficulty of the print. Additionally, the round shape of the shaft creates an overhang on its underside. FFF 3D printing requires

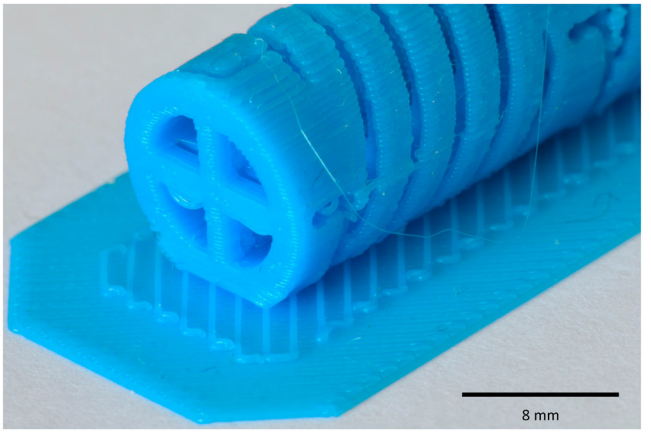

Figure 3. HelicoFlex segment printed horizontally on a raft. The object sits on a series of individual extrusion lines running 45° to the long axis of the shaft. Each line is 0.25 mm thick and is separated from adjacent lines by 0.65 mm.

that each layer is supported by the one below it. While it is possible to print overhangs, the resolution of small features and surface quality of the resulting object will worsen with an increasing overhang. Printing the HelicoFlex on its side results in relatively large overhangs both in a radial direction on the outer surface of the shaft as well as in an axial direction between the individual helicoids. The worst radial overhangs are located in the lower half of the print, which serves as the base for the rest of the print.

Solution: Gentle helix angle

One way of mitigating overhang issues is to reduce the layer height of the 3D print, as the overhangs would then be discretised into thinner slices, meaning each layer also overhangs by a shorter distance. In theory, the Prusa i3 MK3s used in this work is capable of a 0.05 mm layer height, however this would drastically increase print time.

It is difficult to mitigate the overhang in the radial direction, as this overhang is due to the round cross-section of the shaft. Mitigating this overhang would force major changes to the shaft geometry, e.g. making the cross section hexagonal or square, which would negatively affect the functionality of the design. It was instead decided to give the helicoid a lower helix angle to improve printability, the result of which is shown in Figure 4. The lower helix angle reduces the severity of the overhang in the axial direction, which helps reduce the overall disturbance created by the overhanging geometry. This was achieved by increasing the number of turns around the backbone from one to eight (see Figure 4(a)), and reducing the number of intertwined helicoids from four to one. To leave room at the outer edge of the helicoid to allow bending, the width of the helicoids' cross-section at its outer edge was reduced from 1.5 mm to 1.2 mm. This resulted in much fewer print artefacts resulting from unsupported overhangs.

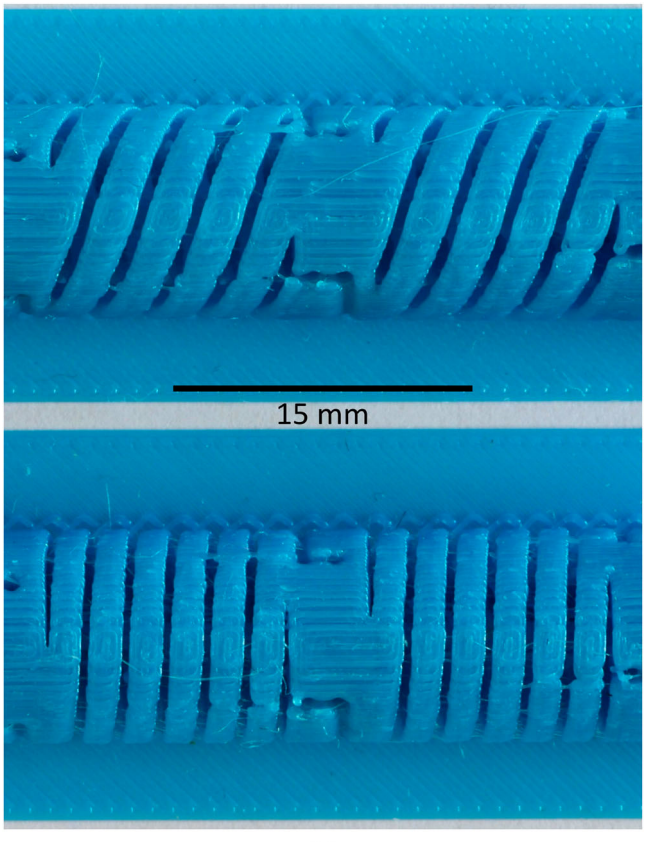

(a)

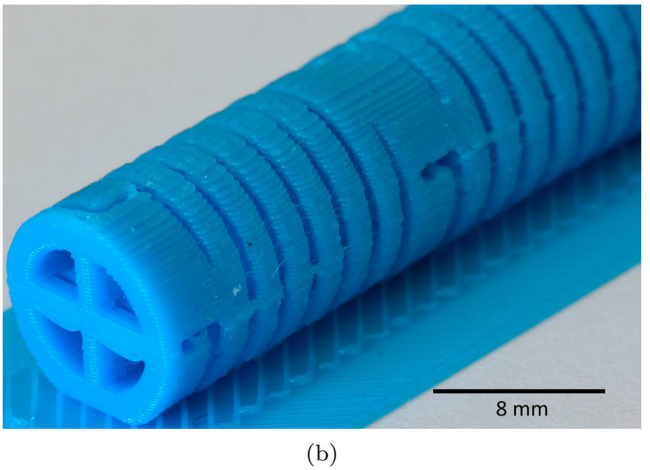

(b)

Figure 4. Managing overhangs by modifying the helix angle. (a): Comparison of old (upper) and new (lower) helicoids. Reducing the number of intertwined helicoids from four to a single one leads to a lower helix angle, which helps reduce overhang artefacts. (b): Overview photograph of a 3D print with the new, single helicoid, low helix angle shaft design.

3.4. Managing thin sections

Problem: Sections too thin for extrusion width

The cross-section of each helicoid in the HelicoFlex features a tapered 'T' shape. The base of the 'T' points to the central axis and narrows to 0.2 mm as it approaches the spine of the shaft. The top of the 'T' makes up the outer surface of the helicoid. This taper reduces bending stiffness by reducing the amount of material that must bend. This strategy works well for DLP printing with its very fine resolution. However, the smallest feature an FFF printer can resolve is its extrusion width - in this study, this is 0.25 mm. The HelicoFlex has many areas where a finer extrusion width is required, particularly around the tendon channels, the fixation points, and the centre of the helicoid. In cases where a feature is smaller than the extrusion width, the slicer will not generate an extrusion, creating gaps for these thin walled areas. This results in tendon fixation points that are not fully enclosed, or small areas where helices are barely attached to the spine of the segment, see Figure 5(a).

Solution: Thin sections as a multiple of extrusions

If an object features thin sections, such as the helicoids of the HelicoFlex, their width should be selected such that no gaps are created between the perimeter extrusions of the feature, as this would weaken the resulting print. Specifically, this means thin walls should be the same width as an integer number of extrusion lines, i.e. the design should be adjusted to the width and spacing of the extrusion lines.

The spacing between extrusion lines is deliberately slightly smaller than the width of the extrusion, fusing adjacent extrusions to one another. Therefore one cannot simply multiply the desired number of extrusions by the extrusion width to determine the right thickness for a thin section. Instead the section thickness is a function of the number of extrusions, their spacing and the extrusion width. Extrusion spacing is derived from extrusion width and layer height using the formula published in the Slic3r manual (Slic3r manual 2022):

$$s = W_e - H_l \cdot \left(1 - \frac{\pi}{4}\right) \tag{1}$$

Where s is the spacing between the paths of adjacent extrusions, W_e is the width of each extrusion line and H_l is the height of each layer. The thickness of a section consisting of n extrusions (where $n \in \mathbb{Z}^+$) is described as:

$$T_s = s \cdot (n - 1) + W_e \tag{2}$$

Where T_s is the thickness of the section. For example, $n = 5$ extrusions at a layer height of $H_l = 0.15$ mm and an extrusion width of $W_e = 0.25$ mm, as used in our design, will yield a section thickness of $T_s = 1.12$ mm.

By changing the profile of the helicoids to a simple rectangle with a width of 1.12 mm, gaps between the helicoids and the spine are avoided entirely. The left side of Figure 5(b) shows a cross-section of the resulting 3D print, and Figure 5(b), right shows a side view displaying the external appearance of the new helicoid structure.

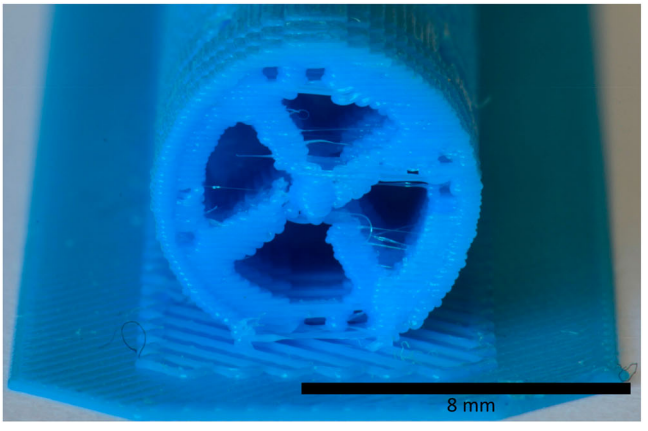

(a)

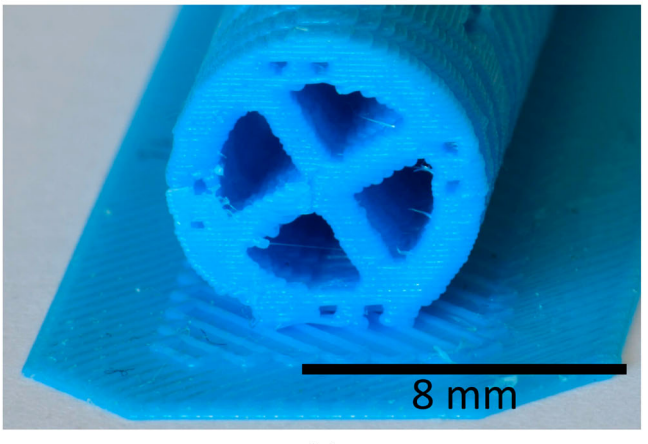

(b)

Figure 5. Managing thin part sections when printing on an FFF printer. (a): cutaway of the HelicoFlex segment introduced in Section 3.3 showing print artefacts due to missing extrusions or gaps near the spine of the shaft. (b): cross-section and side view of a 3D printed shaft using wall thicknesses from Equation (2). Note the absence of gaps or related thin-wall artifacts.

3.5. Managing resolution

Problem: Features too small for print resolution

The HelicoFlex features 20 individual ⌀0.45 mm channels, arranged around the outside of its shaft. During assembly, the tendons must manually be threaded through each channel. However, due to the relatively limited resolution of FFF 3D printers these were unreliable, being either blocked somewhere along their length by stray extrusions or by becoming too narrow to push tendons through, see Figure 6(a), around the circumference of the section.

The poorly resolved channels cause the tendons to fray during threading, which prevents them from passing through their channels and makes it impossible to implement steering.

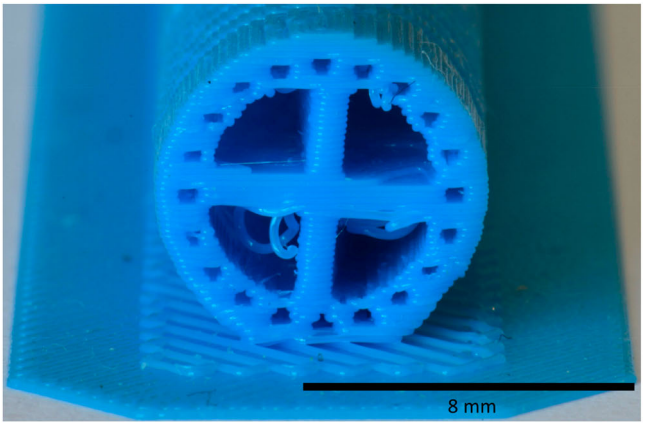

(a)

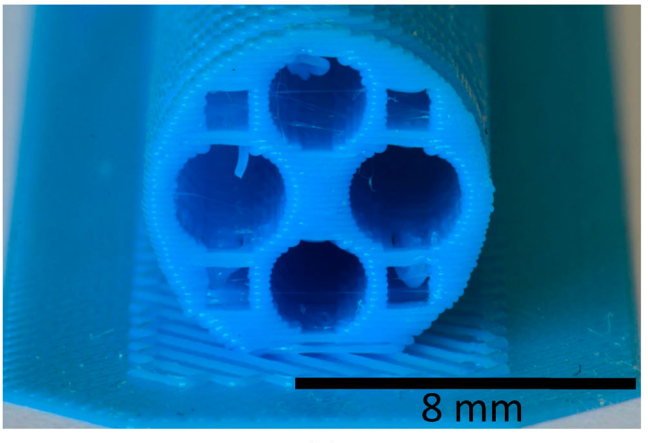

(b)

Figure 6. Combining features to overcome resolution limits. **(a):** Closeup of the proximal end of the 3D print described in Section 3.4 showing the irregular shape of the tendon channels due to the limits of the printer's resolution. (b): 3D printed compliant segment with combined channels. The square channels have a size of 1 mm × 1 mm and guide the tendons, while the circular channels allow the passage of flexible instruments and are 2.2 mm (top and bottom channel) and 2.5 mm (left and right channel) in diameter

Solution: Features combined

The resolution of FFF 3D printers is primarily limited by the consistency of the extrusion being laid down. Most filaments specify tolerances of ±0.05 mm, with more precise filaments specifying ±0.02 mm. This can affect the cross-sectional area, and therefore the extrusion flow rate of a 1.75 mm filament by as much as 5.8%. Furthermore, most FFF materials are hygroscopic to some degree. Absorbed water is converted to steam during printing, expanding and disturbing the flow of plastic from the nozzle, causing localised overextrusion.

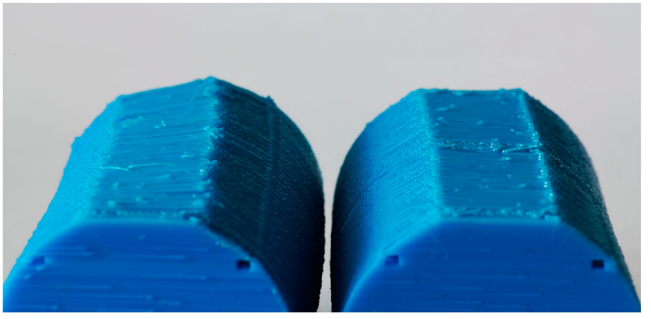

Figure 7. Mirror geometry to prevent warping. Left: A 60 mm long and 26.3 mm diameter 3Flex segment showing the axial twist incurred by contraction of the 3D printed material. Right: a 3Flex segment of the same length and diameter, split into two sections of opposing chirality and thereby largely cancelling the axial twist induced by material shrinkage.

While the original HelicoFlex routed each tendon through its own channel, this is not strictly necessary if each segment is controlled by four tendons spaced 90° apart. To overcome these limitations, the 20 small tendon channels were consolidated into just four larger channels, each with a square size of 1 mm × 1 mm and guiding five tendons, resulting in the 3D print shown in Figure 6(b). Furthermore, the tendon attachment points were simplified into grooves around which the tendon can be looped and knotted into place.

Gathering the tendons in just four channels also created more space for working channels in the shaft. This design possesses two 2.2 mm and two 2.5 mm working channels, increasing the range of usable tools to include standard 2.4 mm endoscopy instruments.

3.6. Managing contraction

Problem: Warped geometry

Warping of the object being printed is a common problem in FFF 3D printing arising out of the thermal contraction of the print material as it cools from its molten state. As this effect is proportional to the overall length of the object it is usually only noticeable in larger objects while being negligible in parts the size of the HelicoFlex, which is only eight mm in diameter. The effective length of the helicoid however, particularly the single-start helicoid introduced in Section 3.3 is significantly longer than the axial length of the segment itself. This means that the helicoid will shorten more than the other dimensions of the shaft with thermal contraction, inducing a twist in the shaft, see Figure 7, left. A twisted helical structure causes the tendons running through the segment channels to no longer run parallel to the axis of the segment, instead giving them a helical path. Ultimately this results in a non-intuitive twist in the tip motion of the instrument relative to the user's control inputs on the handle.

Solution: Mirrored geometry

As the twist induced by thermal contraction is intrinsic to the material being printed and the structure of the part, it is difficult to avoid. The direction of twist is affected by the chirality, i.e. the left- or right-handedness of the helicoid, as it is a result of the helicoid shortening in length and imposing a twist on the overall structure. This fact can be exploited

to average out the twist of a compliant shaft consisting of multiple segments. Right and left handed helicoids that are otherwise identical will shrink and twist by approximately the same amount, albeit in opposite directions. By alternating segments with right and left handed helicoids, each segment will oppose the twist induced by its neighbour, evening out the effect over the length of the shaft. The resulting effect is shown in Figure 7, right.

3.7. Design guideline summary

The process of redesigning the HelicoFlex led to a series of guidelines for the manufacture of complex objects with fine detail on FFF 3D printers. These are summarised below:

(1) *Keep it flat:* objects with a tall and slender aspect ratio are best printed flat on the bed to maximise printbed contact, especially on 3D printers with a moving bed.
(2) *Adhere to lines, not surfaces:* fragile objects are better off adhering to a raft consisting of individual extrusions than the print bed or a solidly filled raft with air gap.
(3) *Use more gentle overhangs:* avoid overhangs entirely or reduce them to a gentler angle. Overhangs worsen surface finish and small detail resolution in overhanging areas is lost.
(4) *Design thin sections as an integer number of extrusions:* the thickness of thin sections should be selected based on Equations (1) and (2) to avoid internal gaps.
(5) *Combine small features:* where possible, avoid resolution problems by merging many small features into one, larger feature that performs the same purpose.
(6) *Mirror geometry to counter warping:* FFF printed parts tend to contract and warp as they cool. By mirroring the geometry of the part, the contraction opposes itself, which prevents warping.

4. Results

4.1. Assembly

The 3Flex is printed in twelve individual pieces that are glued together during assembly. These consist of five tip segments, the converging section, five handle segments, and a cosmetic handle end cap. Post-processing 3Flex segments involves removing the raft material and running a scalpel blade through the helicoid to remove stray pieces of material.

The tendons are threaded through the 3Flex shaft by hand and are looped and knotted into their respective attachment grooves along the shaft. Spectra fishing line with a diameter of 0.19 mm and a rated breaking strength of 128N was chosen as the tendon material owing to its low coefficient of friction and excellent wear resistance. Once the tendons have been threaded through them, adjacent segments are assembled from the distal to the proximal end using cyanoacrylate glue. Each shaft segment has the opposite-handed helix to its distal and proximal neighbours to reduce axial twist, as explained in Section 3.6.

Assembly including raft removal, object cleanup, tendon threading and glue-up took approximately five hours, which is comparable to the time requirements reported in the paper by Culmone et al. (2020).

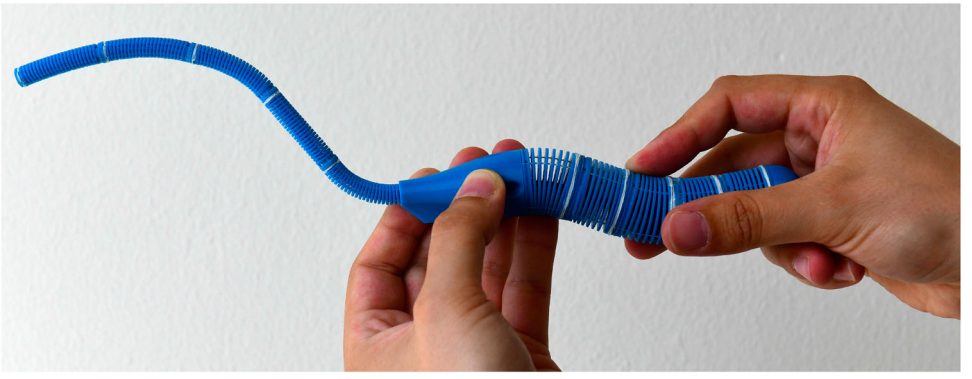

Figure 8. Five-segment multi-steerable instrument based on the 3Flex segment design. Left: the instrument features a 175 mm long and ⌀8 mm steerable shaft with two 2.2 mm and two 2.5 mm working channels. The converging cone in the middle adapts the steerable tip to the flexible handle and allows access to the working channels. Right: the flexible handle of the instrument. The distal tip mirrors the shape of the handle.

4.2. Final 3Flex prototype

The 3Flex is the culmination of applying the guidelines laid out in Section 3.7 to convert the HelicoFlex design to 3D printing with the FFF process. The result is a multi-steerable, tendon actuated flexible instrument similar in capability to the HelicoFlex, printed on a machine that costs less than €1000, shown in Figure 8.

Like the HelicoFlex described in Section 1.2, the shaft has a diameter of eight mm and comprises five steerable segments that can be individually controlled in two DOF by four tendons, resulting in a total of 10 controlled DOF. In the 3Flex, the steerable segments are 35 mm long, for a total steerable length of 175 mm. Furthermore, the shaft possesses four working channels, two of which have a diameter of 2.2 mm and two of which have a diameter of 2.5 mm.

5. Discussion

5.1. Cost and accessibility

The major motivator for this work was to provide a framework of guidelines to take DLP printed parts and convert them to functionally similar or equivalent parts that can be printed using much more affordable FFF printers. While the EnvisionTec Perfactory 4 Mini XL used by Culmone et al. (2020) is a professional-grade printer with an undisclosed price tag, the Prusa i3 MK3S is available as a kit for less than €1000.

Additionally to the price difference, there is a difference in operational requirements between the two processes; a DLP printer requires solvents to clean parts, which require appropriate storage and hazard management, and the EnvisionTec is a floor-standing machine. By comparison, the Prusa is a desktop machine and requires no potentially hazardous chemicals to operate. This combination of financial and operational requirements can easily place DLP printing outside the realm of possibility for small research groups or individuals. In these cases, the guidelines in Section 3 can be especially helpful to achieve

functionally comparable results to DLP printing when designing small, detailed parts in a more restrictive setting.

Printing all of the required components for one instrument as shown in Figure 8 took around 27 hours and 65 g of PLA. The PLA filament used for the prototype retails for €20/kg, translating to €1.30 of material per assembly. Assuming an average power consumption of 80 W means approximately 2.16 kWh of electricity were consumed during the printing process at a price of €0.34/kWh, bringing the total electricity cost to €0.74. Approximately seven meters of tendons (Daiwa J-Braid X8 ⌀0.18 mm dyneema fishing line) were used in the assembly. At a price of €24/300m spool, this added €0.56 to the total bill of materials cost, bringing the final price to €2.60. Approximately six hours of work were required to remove the raft material from the 3D printed parts, thread the tendons through the assembly, glue the parts into place and attach the tendons to their fixation points in the handle. The amount of glue used in the process was not quantified; however this is such a small amount that the impact on the price of the prototype is likely on the order of individual cents.

Culmone et al. do not provide a detailed breakdown of the costs of the prototype, only the printing and assembly times, given as 26 and 5 hours, respectively. While it is difficult to ascertain a price for the R5 resin used in the HelicoFlex, it can be estimated at around €250/kg. The power usage of the Perfactory 4 mini XL is specified at 2.4 A at 230 V, implying a peak power of around 552 W, which at least allows a rough estimate of the electricity cost. Assuming the printer runs in steady state at about half of its maximum power rating means one assembly costs €2.44 in electricity alone. This is already almost the cost of an entire FFF-printed instrument including electricity and tendons.

5.2. Comparison to the HelicoFlex

The key features of the HelicoFlex were its low bending stiffness, the high number of DOF, its ability to include working channels and its 3D printability, which made the design more suited to disposable use than conventionally-manufactured instruments. The 3Flex design achieves the same diameter, number of DOF, a similar bending stiffness, the same number of working channels and is printable on even basic machines. Its main drawback over the HelicoFlex lies in its assembly: While it is possible to 3D print many segments in one contiguous piece in the same way the HelicoFlex is, this makes threading its tendons much harder due to manner in which the tendons are routed in shared rather than discrete channels. It can therefore be argued that design modifications brought about by applying the guidelines described in Section 3 result in a design that is, excusing some minor caveats, functionally comparable to the original while being manufactured using much more affordable tools.

5.3. Comparable Fused Filament Fabrication (FFF)-printed designs

A preliminary literature search showed only two other publications where the steering articulation of surgical instruments were directly printed using the FFF process, those being Hwang and Kwon (2020) and Hernández-Valderrama et al. (2022). Both designs consist of many discretely-printed parts forming a single two-DOF joint that are later assembled. By comparison, the 3Flex requires much less assembly, has a smaller diameter and can be

daisy-chained to create multi-steerable instruments with many DOF. Furthermore, the 3Flex is an open-source, parametric design that can be downloaded and adjusted to the needs of a given project in minutes.

5.4. Durability

Although the 3Flex is printed parallel to the *XY* plane of the printer, pulling on the shaft in the axial direction can lead to failure as the individual turns of the helicoid shear along the layer lines of the 3D print.

This problem is at least partially mitigated by the tendons, which act as tensile reinforcements taking up some of the load and reducing the amount of shear loading on the 3D printed part of the structure. If a break does occur in the structure of the shaft, the tendons ensure that pieces of the shaft remain together, aligned and steering generally continues to function. This is an important advantage from a safety standpoint; should such a device fail during a medical procedure, there is sufficient mechanical integrity to remove this instrument in a controlled manner and either replace the instrument or convert to an open procedure.

5.5. Backlash

While the HelicoFlex design guides each tendon through its own channel, the 3Flex bundles tendons together in just four channels. This is an important adjustment to permit printing the design using the FFF process, but it comes with added backlash. Backlash in tendon-driven manipulators largely comes from radial movement of the tendons during bending. As a segment bends, the tendons in the segment will experience a lateral force towards the inside of the bend, pushing them against the wall of the channel. This lateral movement disrupts the relationship between segment bending and tendon displacement, as it is dependent on the radial distance between the tendon and the neutral axis of the segment, causing backlash.

In the multi-steerable 3Flex shaft, the most proximal segment in the shaft guides all of the tendons connected to the more distal segments, meaning the tendons constrain one another. Each more distal segment will have progressively fewer tendons occupying space in the tendon channel, increasing the room for tendons to move laterally in the channel. This means backlash will progressively worsen along the shaft, with the most backlash at the distal tip of the shaft. One possible mitigation for this issue could be to progressively narrow the tendon channel towards the distal tip of the shaft, reducing the room for lateral tendon movement. However, without careful implementation this could cause the issues described in Section 3.5 to reoccur.

5.6. Friction and wrapped tendons

The tendons are first threaded and knotted into the individual shaft segments, after which the segments are assembled to form the shaft as a whole. As there are multiple tendons in each channel, it is possible that tendons may become wrapped around each other within the channel during assembly. Wrapping increases the normal forces between the tendons, increasing friction and potentially causing unwanted tip bending. Close attention

must be paid during the assembly process to avoid wrapping tendons in this way, as once the shaft is assembled, it is easier to start over than to attempt disassembly and manual disentanglement.

5.7. Towards medical usage

Combining the non-assembly methods developed by Culmone et al. (2020) with the guidelines developed in this paper could produce low cost, yet highly-capable single use instruments for various medical applications. The design can be tailored to suit specific medical applications. For example, by chaining a number of longer segments, it is possible to create a longer multi-steerable device suited for gastrointestinal endoscopy. Alternatively, a single steerable segment placed distally on a rigid shaft could create a wrist-articulated instrument. Furthermore, by simply selecting a biocompatible grade of PLA to 3D print the structure of a device, biocompatibility as well as Magnetic Resonance Imaging (MRI) compatibility can be achieved with relative ease. As FFF 3D printing is capable of producing sterile parts (Neches et al. 2016), with correct handling and packaging the guidelines proposed in this paper can in principle be used to enable 3D printing of low-cost and potentially patient-specific surgical instruments directly in a hospital setting.

6. Conclusion

We converted a design for a 3D printed compliant medical instrument from printing on a Digital Light Processing (DLP) printer to a Fused Filament Fabrication (FFF) printer. The knowledge gained from this process was generalised into six widely applicable guidelines which provide a framework to manage and compensate for differences in the two processes to achieve comparable results at a reduced cost. A FFF 3D printed prototype was created to show that the production of equivalent instruments is possible using a more affordable process than DLP. The resulting device features a 175 mm long shaft with five steerable segments, each independently steerable in two degrees of freedom. The device also features four working channels, two of 2.2 mm and two of 2.5 mm diameter. Devices based on this manufacturing approach could be used to manufacture affordable yet highly articulated single-use instruments for minimally invasive interventions.

Disclosure statement

No potential conflict of interest was reported by the author(s).

Funding

This work was supported by the ATLAS project. This project has received funding from the European Union's Horizon 2020 research and innovation program under the Marie Skłodowska-Curie grant agreement No 813782.

Data availability

The parametric 3Flex design as well as the required 3D printing settings are available from the 4TU.ResearchData repository (Trauzettel et al. 2022) under the Creative Commons Attribution 4.0 International (CC BY 4.0) licence.

References

Ai, X., A. Gao, Z. Lin, C. He, and W. Chen. 2021, July. "A Multi-Contact-Aided Continuum Manipulator With Anisotropic Shapes." *IEEE Robotics and Automation Letters* 6 (3): 4560–4567. https://doi.org/10.1109/LRA.2021.3068648.

Culmone, C., P. W. Henselmans, R. I. van Starkenburg, and P. Breedveld. 2020, May. "Exploring Non-Assembly 3D Printing for Novel Compliant Surgical Devices." *PLoS One* 15 (5): e0232952. https://doi.org/10.1371/journal.pone.0232952.

Culmone, C., K. Lussenburg, J. Alkemade, G. Smit, A. Sakes, and P. Breedveld. 2021, December. "A Fully 3D-Printed Steerable Instrument for Minimally Invasive Surgery." *Materials* 14:7910. https://doi.org/10.3390/ma14247910.

Culmone, C., S. F. Yikilmaz, F. Trauzettel, and P. Breedveld. 2021. "Follow-the-Leader Mechanisms in Medical Devices: A Review on Scientific and Patent Literature." *IEEE Reviews in Biomedical Engineering*. https://ieeexplore.ieee.org/document/9541090/.

Henselmans, P. W., C. Culmone, D. J. Jager, R. I. van Starkenburg, and P. Breedveld. 2020, December. "The Memoflex II, a Non-Robotic Approach to Follow-the-Leader Motion of a Snake-Like Instrument for Surgery Using Four Predetermined Physical Tracks." *Medical Engineering & Physics* 86:86–95. https://doi.org/10.1016/j.medengphy.2020.10.013.

Hernández-Valderrama, V. G., R. M. Ordorica-Flores, S. Montoya-Alvarez, D. Haro-Mendoza, L. Ochoa-Toledo, D. Lorias-Espinoza, J. L. Ortiz-Simón, and F. Pérez-Escamirosa. 2022, June. "Steerable Surgical Instrument for Conventional and Single-Site Minimally Invasive Surgery." *Surgical Innovation* 29 (3): 449–458. https://doi.org/10.1177/15533506211037091.

Hwang, M., and D.-S. Kwon. 2020. "K-FLEX: A Flexible Robotic Platform for Scar-Free Endoscopic Surgery." *The International Journal of Medical Robotics and Computer Assisted Surgery* 16 (2): e2078. https://doi.org/10.1002/rcs.v16.2.

Josef Prusa acquires US-based company Printed Solid, Inc. 2022. [Internet]; https://www.prusa3d.com/article/josef-prusa-acquires-us-basedcompany-printed-solid-inc-_230651/.

Krieger, Y. S., C. -M. Kuball, D. Rumschoettel, C. Dietz, J. H. Pfeiffer, D. B. Roppenecker, and T. C. Lueth. 2017, September. "Fatigue Strength of Laser Sintered Flexure Hinge Structures for Soft Robotic Applications." In *2017 IEEE/RSJ International Conference on Intelligent Robots and Systems (IROS)*, 1230–1235, Vancouver, BC: IEEE.

Lin, D., N. Jiao, Z. Wang, and L. Liu. 2021, April. "A Magnetic Continuum Robot With Multi-Mode Control Using Opposite-Magnetized Magnets." *IEEE Robotics and Automation Letters* 6 (2): 2485–2492. https://doi.org/10.1109/LSP.2016.

Lou, C.-W., C.-H. Yao, Y.-S. Chen, T.-C. Hsieh, J.-H. Lin, and W.-H. Hsing. 2008, November. "Manufacturing and Properties of PLA Absorbable Surgical Suture." *Textile Research Journal* 78 (11): 958–965. https://doi.org/10.1177/0040517507087856.

Mohiuddin, K., and S. J. Swanson. 2013. "Maximizing the Benefit of Minimally Invasive Surgery." https://pubmed.ncbi.nlm.nih.gov/24037974/.

Neches, R. Y., K. J. Flynn, L. Zaman, E. Tung, and N. Pudlo. 2016. "On the Intrinsic Sterility of 3D Printing." *PeerJ* 2016. https://peerj.com/articles/2661/.

Scheltes, J. S. 2019. "European Patent ep3752078b1: Surgical Instrument with Mechanically Operable Lever." https://worldwide.espacenet.com/patent/search?q = pn%3DEP3752078B1.

Slic3r manual. 2022. Flow math [internet]. https://manual.slic3r.org/advanced/flow-math.

Song, D., S. Wang, Z. Zhang, X. Yu, and C. Shi. 2023, August. "A Novel Continuum Overtube With Improved Triangulation for Flexible Robotic Endoscopy." *IEEE Transactions on Medical Robotics and Bionics* 5 (3): 657–668. https://doi.org/10.1109/TMRB.2023.3294527.

Sorokin, I., N. E. Canvasser, B. Irwin, R. Autorino, E. N. Liatsikos, J. A. Cadeddu, and A. Rane. 2017, October. "The Decline of Laparoendoscopic Single-Site Surgery: A Survey of the Endourological Society to Identify Shortcomings and Guidance for Future Directions." *Journal of Endourology* 31:1049–1055. https://doi.org/10.1089/end.2017.0280.

Teoh, A. Y. B., S. M. Chan, H. C. Yip, V. W. Y. Wong, P. W. Y. Chiu, and E. K. W. Ng. 2018, March. "Randomized Controlled Trial of Endowrist-Enabled Robotic Versus Human Laparoendoscopic

Single-Site Access Surgery (LESS) in the Porcine Model." *Surgical Endoscopy* 32 (3): 1273–1279. https://doi.org/10.1007/s00464-017-5803-7.

Trauzettel, F., E. Vander Poorten, M. Ourak, J. Dankelman, and P. Breedveld. 2022. "3flex – 3D Printable Parametric Tendon-Driven Manipulator." https://doi.org/10.4121/21666116.

Vliet, W. J. V. D., L. N. Spaans, D. S. Bonouvrie, M. Uittenbogaart, and W. K. Leclercq. 2022, April. "Safety and Efficiency of an Articulating Needle Driver in Advanced Laparoscopic Abdominal Surgery." *Journal of Laparoendoscopic and Advanced Surgical Techniques* 32 (4): 422–426. https://doi.org/10.1089/lap.2021.0272.

Wang, Z., S. Bao, D. Wang, S. Qian, J. Zhang, and M. Hai. 2023, December. "Design of a Novel Flexible Robotic Laparoscope Using a Two Degrees-of-Freedom Cable-Driven Continuum Mechanism With Major Arc Notches." *Journal of Mechanisms and Robotics* 15 (6): 064502. https://doi.org/10.1115/1.4056502.

Wu, D., J. Li, D. Song, Z. Zhang, K. Wang, and C. Shi. 2023, May. "Development of a Novel Ball-and-Socket Flexible Manipulator for Minimally Invasive Flexible Surgery." *IEEE Transactions on Medical Robotics and Bionics* 5 (2): 278–288. https://doi.org/10.1109/TMRB.2023.3265714.